Robotica (2015) volume 33, pp. 1973–1983. © Cambridge University Press 2014
doi:10.1017/S0263574714001209

Optimization of a redundantly actuated 5R symmetrical parallel mechanism based on structural stiffness

Sangrok Jin†, Jongwon Kim†*, and TaeWon Seo‡*

†*School of Mechanical and Aerospace Engineering, Seoul Nat'l University, Seoul 151-019, Republic of Korea*
‡*School of Mechanical Engineering, Yeungnam University, Gyeongsan 712-749, Republic of Korea*

(Accepted April 18, 2014. First published online: May 15, 2014)

SUMMARY
A redundantly actuated parallel kinematic machine (PKM) can be used to avoid singularities, normalize manipulability, and increase the stiffness of anon-redundant mechanism. In this study, a redundantly actuated symmetrical PKM with five revolute (5R) joints is optimized for isotropic stiffness in the workspace. The stiffness of the 5R symmetrical PKM is calculated by the superposition of the actuator stiffness and the structural stiffness. We compared the stiffness of anon-redundant PKM and a redundant PKM. Compliance ellipses of the actuator stiffness and the structural stiffness of the non-redundant PKM resulted in the same configurations in the workspace, while those of the redundant PKM resulted in very different configurations. Optimization was performed by determining the optimal actuator torques that are needed to maximize the conditioning index. Optimal results considering structural stiffness can provide a more uniform directional stiffness than optimal results considering the index. When the strength of the linkages in a PKM is weak, the structural stiffness affects the actual stiffness considerably. We believe that the results of this study can be used to help design and control redundant PKMs.

KEYWORDS: Parallel mechanism; Redundant actuation; Optimization; Stiffness analysis, Structural stiffness.

Nomenclature

Symbol	Definition	Symbol	Definition
r_i	Length of linkage	U_i	Virtual work
θ_i	Joint angle	A	Cross sectional area
θ_p	Joint angle of end effector	E	Modulus of elasticity
$\boldsymbol{q} = [\theta_1\theta_2\theta_3\theta_4]^T$	Joint angle vector	I	Area moment of inertia
$\boldsymbol{q}_u = [\theta_1\theta_2]^T$	Independent joint angle vector	K_{act}	Actuator stiffness
$\boldsymbol{q}_v = [\theta_3\theta_4]^T$	Dependent joint angle vector	K_{active}	Active stiffness
$\boldsymbol{q}_r$	Driving joint angle vector	K_{passive}	Passive stiffness
$\boldsymbol{x} = [x\,y]^T$	Position of end effector	K_{r}	Rotational stiffness of driving joint
$\boldsymbol{J}$	Inverse Jacobian	K_{str}	Structural stiffness
Γ, Φ, Ψ	Constraint Jacobians	K_{total}	End effector stiffness
$\boldsymbol{\tau}_r$	Driving torque	C_{str}	Compliance matrix
$f = [f_x\,f_y]^T$	External force to the end effector	σ_i	Singular value of stiffness matrix

* Corresponding author. E-mail: jongkim@snu.ac.kr, taewon_seo@yu.ac.kr

https://doi.org/10.1017/S0263574714001209 Published online by Cambridge University Press

Symbol	Definition	Symbol	Definition
R_i	Reaction force of a linkage	I	Index number
C_i	Compression force of a linkage	I_{con}	Index number considering structural stiffness
V_i	Vending force of a linkage	I_{ign}	Index number ignoring structure stiffness
M_i	Moment of a linkage	R	Dimensionless number to evaluate the influence of actuation torque for the linkage strength

1. Introduction

Parallel kinematic machines (PKMs) have been widely researched for applications in haptic devices, motion simulators, and positioning devices.[1,2] Theoretically, PKMs should have advantages of high resolution, high precision, and high stiffness.[3] However, in practice, their low stiffness limits their applicability in areas such as machining centers and robot manipulators.[4] The low stiffness in assembled PKMs is attributed to too many joints, assembly errors, and thinner links than those used in serial mechanisms.

Several studies have been performed to adjust the stiffness of PKMs by changing the design of the mechanism or its actuation process. Zhang[5] proposed a new parallel mechanism by changing the joint in the base and the end effector of a Tricept mechanism. Wu *et al.*[6] added redundant links on a 2-degree-of-freedom (DOF) PKM to increase the x- and z-directional stiffness for the milling process. Besides changing the design of the mechanism, the stiffness of a PKM can be adjusted by using more actuators than the number of DOFs of the PKM (so-called "redundant actuation"). Chakarov[7] detailed the derivation of the antagonistic stiffness of a redundantly actuated PKM, which can be changed by using the null space torque of the actuators. Lee *et al.*[8] optimized the antagonistic stiffness for both uniform distribution and maximum value in a certain direction, and verified the effect of redundant actuation by experiments.

Besides modifying the stiffness, redundant actuation offers manipulability and singularity avoidance.[1,4] Generally, in redundant actuation, actuator torques remain in an equilibrium state without movement. In this case, internal preloads are induced from the actuator torques on the joints and links.[9] Note that the internal preloads affect link deflection. If the links of the PKM are relatively thin,[10,11] redundant actuation will dominantly affect the deflections of the links.

The design of redundant PKMs has been optimized to adjust their stiffness or to increase the workspace. Shin *et al.*[12] optimized a redundant PKM to enhance the stiffness of the end effector while enlarging the workspace of a PKM by using the Taguchi methodology. Lee *et al.*[8] optimized a redundant PKM by using the conditioning index of the stiffness matrix and the maximum stiffness, respectively. In this case, the conditioning index is a popular index for optimization because it can describe the directional uniformity of the stiffness of a PKM.[13] However, to our knowledge, there has been no stiffness analysis of redundant PKMs considering link stiffness, which is very important because PKMs have thin links.

In this study, internal torque based on the stiffness of a redundant PKM is optimized. A five revolute (5R) joint symmetrical PKM is used for the analysis.[14] We superposed structural stiffness with actuator stiffness to determine the stiffness of the end effector.[15] Based on the stiffness analysis, the torques of the PKM were optimized to maximize the conditioning index. The optimization results are compared with the results based on ignoring structural stiffness. Non-redundant and redundant cases are also compared to analyze the effect of the structural stiffness on the final stiffness of the mechanism. The results show why the structural stiffness should be included when optimizing redundant PKMs.

The remainder of the paper is organized as follows. In Section 2, we derive the kinematics of a non-redundant and redundant 5R PKM. In Section 3, we present the stiffness of the non-redundant and redundant PKMs by considering both the actuator stiffness and structural stiffness. Also in this section, stiffness distributions are compared and analyzed. Section 4 presents the optimization

https://doi.org/10.1017/S0263574714001209 Published online by Cambridge University Press

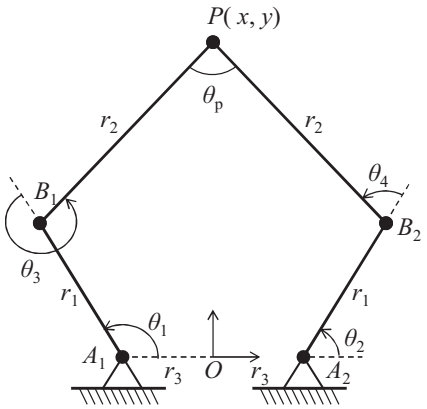


Fig. 1. Geometrical configuration of the 5R symmetrical PKM.

procedure and results for the non-redundant and redundant cases. Concluding remarks are given in Section 5.

2. Configuration and Kinematics of 5R Symmetrical PKM

2.1. Geometric configuration

The 5R parallel mechanism is a 2-DOF mechanism comprised of two independent joints and two dependent joints. As shown in Fig. 1, the lengths of the symmetric links are $\overline{A_1B_1} = \overline{A_2B_2} = r_1$, $\overline{B_1P} = \overline{B_2P} = r_2$, $\overline{OA_1} = \overline{OA_2} = r_3$, which satisfy the conditions of the maximum usable workspace such that $r_3 < r_1 < r_2$, $r_1 + r_3 < r_2$.[14] Joints A_1, A_2 are independent joints and joints B_1, B_2 are dependent joints. P is a point on the end effector. When the model is in the up-configuration (in which the joint angle of the end effector (θ_p) is always acute), the position of P is determined uniquely along the angles of the independent joints θ_1, θ_2.

2.2. Kinematics and Jacobian of the non-redundant case

Constraint equations between an independent joint and the end effector can be written as follows:

$$(x - r_1 \cos\theta_1 + r_3)^2 + (y - r_1 \sin\theta_1)^2 = r_2^2, \tag{1}$$

$$(x - r_1 \cos\theta_2 - r_3)^2 + (y - r_1 \sin\theta_2)^2 = r_2^2. \tag{2}$$

Differentiating the constraint equations with respect to time yields the Jacobian:

$$\dot{\boldsymbol{q}} = \begin{bmatrix} \dot{\theta}_1 \\ \dot{\theta}_2 \end{bmatrix} = A^{-1} B \begin{bmatrix} \dot{x} \\ \dot{y} \end{bmatrix} = J \begin{bmatrix} \dot{x} \\ \dot{y} \end{bmatrix} = J\,\dot{\boldsymbol{x}}, \tag{3}$$

where

$$A = \begin{bmatrix} r_1 y \cos\theta_1 - r_1 (x + r_3) \sin\theta_1 & 0 \\ 0 & r_1 y \cos\theta_2 - r_1 (x - r_3) \sin\theta_2 \end{bmatrix},$$

$$B = \begin{bmatrix} x - r_1 \cos\theta_1 + r_3 & y - r_1 \sin\theta_1 \\ x - r_1 \cos\theta_2 - r_3 & y - r_1 \sin\theta_2 \end{bmatrix}.$$

Where J is the inverse Jacobian, $\boldsymbol{q}$ is the vector of a joint angle, and x is the position vector of the end effector.

2.3. Kinematics and Jacobian of the redundant case

The redundant mechanism has surplus actuators at the dependent joints that generate internal forces. Two surplus actuators are added in joints B_1 and B_2 to change the stiffness topology, while

https://doi.org/10.1017/S0263574714001209 Published online by Cambridge University Press

one-redundancy is proven to affect only the value of stiffness.[8] Constraint equations must involve the angles of the dependent joints. Considering a dependent joint, the constraint equations can be derived as follows:

$$g_1(\theta_1, \theta_2, \theta_3, \theta_4) = r_1 \cos\theta_1 - r_3 + r_2 \cos(\theta_1 + \theta_3) - r_1 \cos\theta_2 - r_3 - r_2 \cos(\theta_2 + \theta_4) = 0, \quad (4)$$

$$g_2(\theta_1, \theta_2, \theta_3, \theta_4) = r_1 \sin\theta_1 + r_2 \sin(\theta_1 + \theta_3) - r_1 \sin\theta_2 - r_2 \sin(\theta_2 + \theta_4) = 0. \quad (5)$$

When the preceding constraint equations are differentiated with respect to time, the constraint Jacobian Φ between the independent joints and the dependent joints is obtained as follows:

$$\frac{\partial g}{\partial q}\dot{q} = \begin{bmatrix} \frac{\partial g_1}{\partial \theta_1} & \frac{\partial g_1}{\partial \theta_2} & \frac{\partial g_1}{\partial \theta_3} & \frac{\partial g_1}{\partial \theta_4} \\ \frac{\partial g_2}{\partial \theta_1} & \frac{\partial g_2}{\partial \theta_2} & \frac{\partial g_2}{\partial \theta_3} & \frac{\partial g_2}{\partial \theta_4} \end{bmatrix} \begin{bmatrix} \dot{\theta}_1 \\ \dot{\theta}_2 \\ \dot{\theta}_3 \\ \dot{\theta}_4 \end{bmatrix} = [\, G_u \quad G_v \,] \begin{bmatrix} \dot{q}_u \\ \dot{q}_v \end{bmatrix} = 0, \quad (6)$$

$$\Phi = -G_v^{-1} G_u, \quad (7)$$

where $\boldsymbol{q}_u$ is the independent joint vector consisting of angles θ_1, θ_2, and $\boldsymbol{q}_v$ is the dependent joint vector consisting of angles θ_3, θ_4. Our definitions of independent and dependent joints are taken from ref. [4] to define the independent variables for the kinematics. The dependent joint vectors are uniquely determined from the independent joint values using Eq. (7).

The driving joint must be determined. In this paper, surplus actuators are attached at all dependent joints. Therefore, the driving joint vector $\boldsymbol{q}_r = [\theta_1, \theta_2, \theta_3, \theta_4]^T$ can be calculated from the constraint Jacobian Γ, which is the relation between an independent joint and a driving joint and can be written as

$$\dot{\boldsymbol{q}}_r = \Gamma \dot{\boldsymbol{q}}_u = \begin{bmatrix} I_{2\times 2} \\ \Phi \end{bmatrix} \dot{\boldsymbol{q}}_u. \quad (8)$$

3. Stiffness Analysis of Non-redundant and Redundant Cases

The stiffness of the end effector according to external forces can be obtained by the superposition of the actuator stiffness K_{act} and the structural stiffness K_{str}, as series-connected springs. The final stiffness matrix K_{total} can be written as

$$\boldsymbol{f} = \left(K_{\text{act}}^{-1} + K_{\text{str}}^{-1}\right)^{-1} \Delta \boldsymbol{x} = K_{\text{total}} \Delta \boldsymbol{x}. \quad (9)$$

3.1. Non-redundant case

3.1.1. Actuator stiffness. The actuator stiffness is obtained by applying the virtual work theorem. When driving torques are operated and the external force is applied at the end effector, a small displacement of the end effector and driving joint is generated. The force and displacement relation is given by

$$\boldsymbol{\tau}^T \Delta \boldsymbol{q} + \boldsymbol{f}^T \Delta \boldsymbol{x} = 0, \quad (10)$$

where $\boldsymbol{\tau}$ is the driving torque, $\boldsymbol{f}$ is the external force, $\Delta \boldsymbol{x}$ is the small displacement of point P, and $\Delta \boldsymbol{q}$ is the small displacement of a joint. In the non-redundant case, the actuator stiffness is determined passively according to the rotational stiffness K_r of the driving joint. By substituting Eq. (3) in Eq. (10), the actuator stiffness matrix can be obtained as follows:

$$\boldsymbol{f} = J^T(-\boldsymbol{\tau}) = J^T K_{\text{r}} J \Delta \boldsymbol{x} = K_{\text{act}} \Delta x. \quad (11)$$

https://doi.org/10.1017/S0263574714001209 Published online by Cambridge University Press

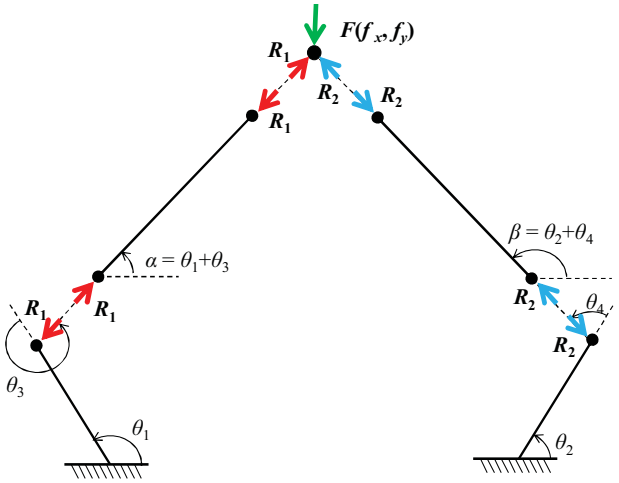


Fig. 2. Free body diagram used to calculate the structural stiffness of a non-redundant case.

3.1.2. Structural stiffness. In order to calculate structural stiffness, the 5R parallel mechanism should be regarded as a truss structure. Both ends of $\overline{B_i P}$ linkages are considered to be pin joints without moments. The rotational stiffness of the driving joints was already considered in the actuator stiffness. Therefore, $\overline{A_i B_i}$ linkages were considered to be cantilever beams. For an arbitrary external force applied at point P in an arbitrary configuration of a 5R PKM, the resulting free body diagram (FBD) about the reaction force is shown in Fig. 2.

Using the force equilibrium equation at point P, reaction forces R_1, R_2 are derived as

$$R_1 = \frac{1}{\sin(\alpha - \beta)}[\sin\beta \quad -\cos\beta]\begin{bmatrix} f_x \\ f_y \end{bmatrix}, \tag{12}$$

$$R_2 = \frac{1}{\sin(\alpha - \beta)}[-\sin\alpha \quad \cos\alpha]\begin{bmatrix} f_x \\ f_y \end{bmatrix}, \tag{13}$$

where $\alpha = \theta_1 + \theta_3$ and $\beta = \theta_2 + \theta_4$.

Only compression occurs in the $\overline{B_i P}$ linkages because there are no moments at either end. The virtual energies U_1, U_2 of corresponding linkages $\overline{B_1 P}$, $\overline{B_2 P}$ respectively, can be derived as follows:

$$U_1 = \frac{R_1^2 r_2}{2AE} \quad \text{and} \quad U_2 = \frac{R_2^2 r_2}{2AE}, \tag{14}$$

where A is the cross sectional area and E is the modulus of elasticity.

In the $\overline{A_i B_i}$ linkages, since these linkages are considered to be cantilever beams, the virtual energies U_3, U_4 of corresponding linkages $\overline{A_1 B_1}$, $\overline{A_2 B_2}$, respectively, can be written as

$$U_3 = \frac{(R_1\cos\theta_3)^2 r_1}{2AE} + \frac{(R_1\sin\theta_3)^2 r_1^3}{6EI}, \tag{15}$$

$$U_4 = \frac{(R_2\cos\theta_4)^2 r_1}{2AE} + \frac{(R_2\sin\theta_4)^2 r_1^3}{6EI}, \tag{16}$$

where I is the second moment of area.

Differentiation of the sum of virtual energies with respect to force gives the compliance matrix based on Castigliano's theorem. This relation is as follows:

$$\frac{\partial U_{\text{total}}}{\partial F} = C_{\text{str}}\begin{bmatrix} f_x \\ f_y \end{bmatrix} = \begin{bmatrix} \Delta x \\ \Delta y \end{bmatrix}. \tag{17}$$

https://doi.org/10.1017/S0263574714001209 Published online by Cambridge University Press

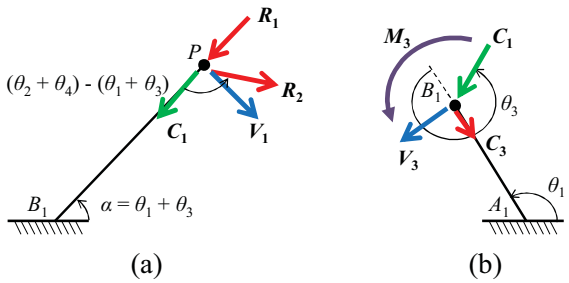


Fig. 3. Free body diagram used to calculate the structural stiffness of a redundant case: (a) $\overline{B_1P}$; (b) $\overline{A_1B_1}$.

The structural stiffness matrix is the inverse of the compliance matrix. Structural stiffness K_{str} of the non-redundant 5R PKM can be obtained as follows:

$$\boldsymbol{f} = C_{\text{str}}^{-1}\Delta\boldsymbol{x} = K_{\text{str}}\Delta\boldsymbol{x}. \tag{18}$$

3.2. Redundant case

3.2.1. Actuator stiffness. Even in the redundant case, the actuator stiffness is obtained using the virtual work theorem. When the driving joint torque is $\boldsymbol{\tau}_r$, the external force is $\boldsymbol{f}$, the displacements of the joint and end effector are $\delta\boldsymbol{q}_r$ and $\delta\boldsymbol{x}$, respectively, and their relational equation is given by

$$\boldsymbol{\tau}_r^T\delta\boldsymbol{q}_r + \boldsymbol{f}^T\delta\boldsymbol{x} = 0. \tag{19}$$

Then, the relation between the external force and the driving torques, Eq. (20), can be derived by substituting Eq. (3) of the inverse Jacobian and Eq. (8) of the constraint Jacobian into Eq. (19) as follows:

$$\boldsymbol{f} = (\Gamma J)^T(-\tau_r) = \Psi^T(-\tau_r). \tag{20}$$

The actuator stiffness matrix in the redundant case is obtained by differentiation of the external force with respect to displacement as follows:

$$K_{\text{act}} = \frac{\partial F}{\partial x} = H^T \otimes (-\tau_r) + \Psi^T K_r \Psi = K_{\text{active}} + K_{\text{passive}}, \tag{21}$$

where $H^T = \frac{\partial \Psi^T}{\partial x}$ and $\otimes$ is the Leibniz product. In the redundant case, the actuator stiffness consists of active stiffness and passive stiffness. Passive stiffness is determined by the rotational stiffness of the joints passively, but active stiffness can be controlled by the driving torques.

3.2.2. Structural stiffness. In redundant cases, moments occur at dependent joints B_i because of the surplus actuators. Joints B_i are not pin joints. Linkages $\overline{B_iP}$ and $\overline{A_iB_i}$ are considered to be cantilevers. Figure 3 shows the FBD of linkages $\overline{B_1P}$ and $\overline{A_1B_1}$.

Reaction forces R_1, R_2 at point P are the same as those of the non-redundant case. As shown in Fig. 3(a), joint B_1 of linkage $\overline{B_1P}$ is clamped, and the linkage is subjected to compression and bending. The compression force and bending force that affect linkage $\overline{B_1P}$ can be written as follows:

$$\text{Compression}: C_1 = R_1 + R_2\cos((\theta_2+\theta_4)-(\theta_1+\theta_3)), \tag{22}$$

$$\text{Bending}: V_1 = R_2\sin((\theta_2+\theta_4)-(\theta_1+\theta_3)). \tag{23}$$

The virtual energy of this linkage is obtained as follows:

$$U_1 = \frac{C_1^2 r_2}{2AE} + \frac{V_1^2 r_2^3}{6EI}. \tag{24}$$

https://doi.org/10.1017/S0263574714001209 Published online by Cambridge University Press

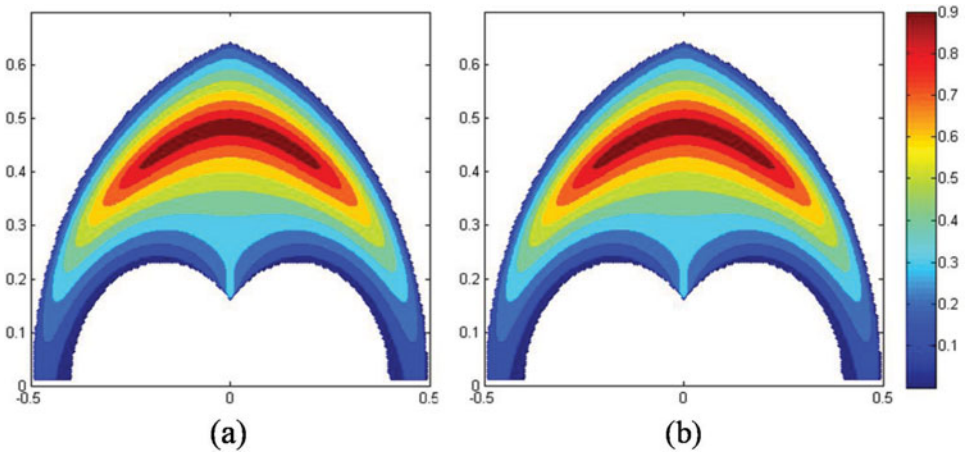


Fig. 4. Stiffness index map of non-redundant 5R PKM: (a) actuator stiffness; (b) structural stiffness.

In linkage $\overline{A_1B_1}$, a moment is generated additionally because joint B_1 is clamped by the actuator. As shown in Fig. 3(b), the reaction force against the compression force C_1 from linkage $\overline{B_1P}$ is decomposed into compression force C_3 and bending force V_3. Moment M_3 is generated by bending force V_1 from linkage $\overline{B_1P}$. The preceding relations are arranged as follows:

$$\text{Compression}: C_3 = C_1 \cos\theta_3, \tag{25}$$

$$\text{Bending}: V_3 = -C_1 \sin\theta_3, \tag{26}$$

$$\text{Moment}: M_3 = V_1 r_2. \tag{27}$$

The virtual energy of linkage $\overline{A_1B_1}$ is derived as follows:

$$U_3 = \frac{1}{2EI}\left(\frac{V_3^2 r_1^3}{3} - V_3 M_3 r_1^2 + M_3^2 r_1\right) + \frac{C_3^2 r_1}{2AE}. \tag{28}$$

Virtual energies U_2, U_4 of linkages $\overline{B_2P}$ and $\overline{A_2B_2}$ can be obtained in the manner described above. The structural stiffness is derived using Castigliano's theorem (e.g., Eqs. (17) and (18)).

3.3. Results

When an arbitrary external force $\boldsymbol{f}$ is applied at end effector point P, the displacement of the end effector is occurs in the direction of the external force. If we draw the point set of displacements for a unit external force, the points are distributed elliptically on the xy plane. This means that the stiffness has directivity. The length of the major axis and minor axis of this ellipse can be substituted with singular values of the stiffness matrix. The ratio of the singular values (I), called the condition number, is an index that expresses the isotropy of the stiffness:

$$\mathrm{I} = \frac{\sigma_2}{\sigma_1}, \tag{29}$$

where σ_1 and σ_2 are singular values of stiffness matrix ($\sigma_1 > \sigma_2$). The isotropy index is popularly used in stiffness research such asin refs. [6], [8], and [13] since the index is meaningful in applications related to robotic manipulation and haptic devices. We note that the size of the stiffness ellipse can be adjusted by changing the actuator torque limit and kinematic parameters of linkages.

In the non-redundant case, the I distribution of structural stiffness is coincident with the I of actuator stiffness, as shown in Fig. 4. Although actuator stiffness and structural stiffness are obtained from different equations, the I indices show exactly the same distributions, as shown in Fig. 4.

https://doi.org/10.1017/S0263574714001209 Published online by Cambridge University Press

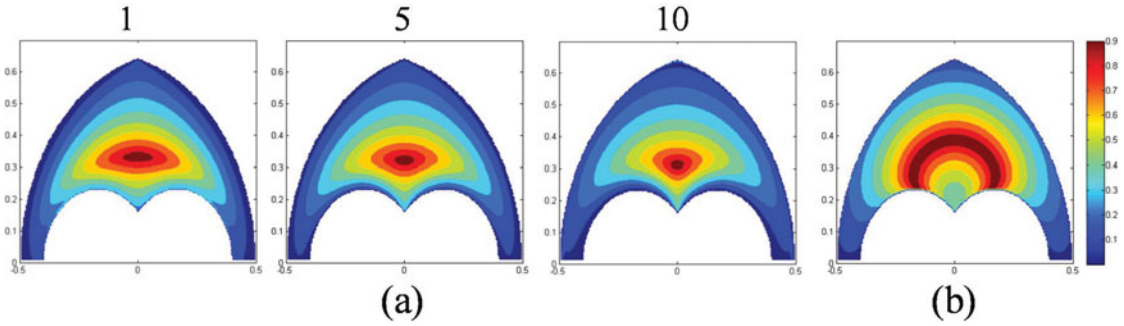


Fig. 5. Stiffness index map of redundant 5R PKM: (a) actuator stiffness; (b) structural stiffness.

In the redundant case, active stiffness can be controlled by additional driving torques. Actuator stiffness can vary, but structural stiffness is determined passively by the configuration of the model. Consequently, the I index for structural stiffness is quite different from that of actuator stiffness, as shown in Fig. 5. Figure 5(a) shows the I distribution of actuator stiffness wherein the driving torques of the independent joints are 5 N m, and the driving torques of the dependent joints are 1, 5, and 10 N m. Figure 5(b) shows the I distribution of the structural stiffness.

In the non-redundant case, the superposition of actuator stiffness and structural stiffness does not affect the distribution of stiffness because I, which indicates the directivity of stiffness, coincides with the actuator stiffness and structural stiffness. In the redundant case, the distributions of actuator stiffness and structural stiffness show a considerable difference. Therefore, a superposition on actuator stiffness and structural stiffness would result in a new distribution of stiffness. In order to analyze the stiffness of a redundant parallel mechanism exactly, the actuator stiffness and structural stiffness need to be analyzed simultaneously.

4. Optimization

4.1. Problem definition

Redundant parallel mechanisms control the distribution of stiffness by internal torques. Uniform stiffness against an arbitrary directional external force is a very important property of the mechanism, and index I expresses this property. In this study, the target model is the 5R PKM. Four actuators are attached at two independent joints and two dependent joints. The optimization of the internal torques makes the compliance ellipse of stiffness a circular shape. A sampling path is drawn from the workspace, and optimization is performed at seven points on the path, which are shown in Fig. 6. Considering the structural stiffness, the optimization finds the optimal torque of each joint to maximize index I, which is the singular value ratio of the end effector stiffness, K_{total}. By ignoring the structural stiffness, the optimization maximizes I for only the actuator stiffness, K_{act}. Compliance ellipses from the optimal torques considering structural stiffness are compared with the results that were obtained without considering structural stiffness.

The maximization of I, which is the ratio of singular values of the stiffness matrix, is the objective function. The maximum value of I is 1, which means the stiffness is isotropic and the compliance ellipse is circular. Driving torque is limited by the power capacity of the actuator. In this study, the maximum driving torque is 10 N m. The optimization problem can be arranged as follows:

$$\begin{aligned} &\text{maximize I} = f\,(x, y, \tau_1, \tau_2, \tau_3, \tau_4), \\ &\text{subject to } \tau_1, \tau_2, \tau_3, \tau_4 \leq \tau_{\max}. \end{aligned} \tag{30}$$

The weaker the structure, the more important the structural stiffness becomes. Given a sufficiently robust structure, structural stiffness does not affect the total stiffness significantly. To evaluate the effect of actuation torque according to the strength of a linkage, a dimensionless number is defined as follows:

$$\text{R} = \frac{\tau_{\max} r}{EI}, \tag{31}$$

https://doi.org/10.1017/S0263574714001209 Published online by Cambridge University Press

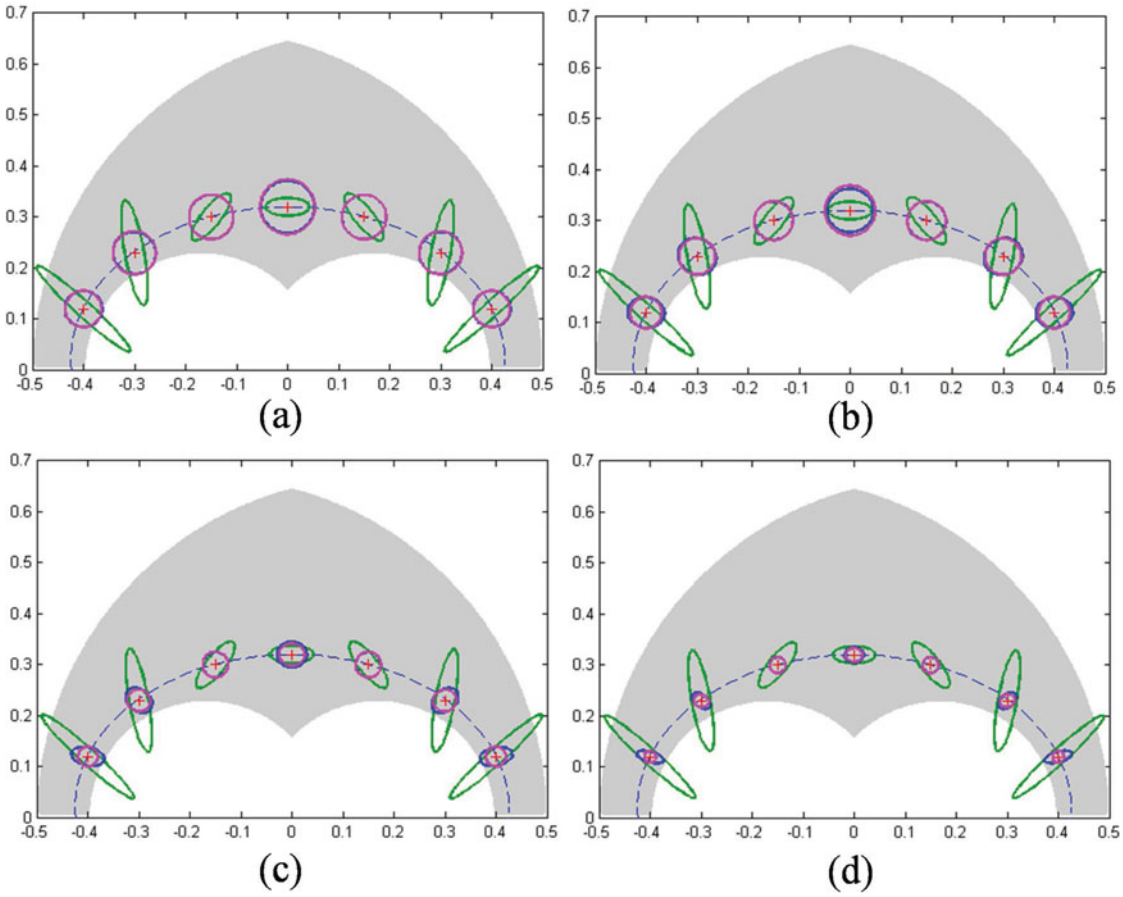


Fig. 6. Optimized stiffness ellipsoids: (a) R = 0.0244, (b) R = 0.0975, (c) R = 0.3901; (d) R = 0.8778.

Table I. Geometric parameters to be used in the optimization.

Length of linkages	Maximum driving torque	Driving joint stiffness
$r_1 = 0.224$ m $r_2 = 0.448$ m $r_3 = 0.168$ m	$\tau_{max} = 10$ N m	$k_r = 10$ N m/rad

Table II. Four different parameters for the optimization.

Parameter	Symbol	R = 0.0244	R = 0.0975	R = 0.3901	R = 0.8778
Cross sectional area	A (m^2)	6×10^{-4}	3×10^{-4}	1.5×10^{-4}	1×10^{-4}
Modulus of elasticity	E (N/m^2)	68.9×10^9	68.9×10^9	68.9×10^9	68.9×10^9
Second moment area	I (m^4)	1×10^{-8}	2.5×10^{-9}	6.25×10^{-10}	2.78×10^{-10}

where τ_{max} is the maximum driving torque and r is the reference length of a linkage. A reference length is the sum of the lengths of the whole linkage. This constant shows the strength of the linkage compared with the driving torque. The greater the value of R, the weaker the structure. The maximum driving torque was fixed at 10 N m, and four cases of structural stiffness were analyzed and compared. The length of each linkage was fixed, and the cross sectional area, modulus of elasticity, and area moment of inertia differ for each case. Parameters used in the optimization are given in Tables I and II. The kinematic variables were chosen to have a relatively large workspace for the 5RPKM.[14] The area moment of inertia in Table II was determined from the area and the geometric shape of the cross section of a linkage.

https://doi.org/10.1017/S0263574714001209 Published online by Cambridge University Press

Table III. Comparison of optimized results..

Position		R = 0.0244			R = 0.0975		
x	*y*	I_{con}	I_{ign}	Difference (%)	I_{con}	I_{ign}	Difference (%)
–0.4	0.12	0.999998	0.945119	5.49	0.999998	0.814402	18.56
–0.3	0.23	1	0.96706	3.29	0.999997	0.888018	11.20
–0.15	0.3	0.999999	0.995996	0.40	0.999999	0.986089	1.39
0	0.32	0.999999	0.978567	2.14	0.998651	0.928971	6.98
0.15	0.3	0.999999	0.995995	0.40	1	0.986088	1.39
0.3	0.23	0.999996	0.967062	3.29	0.999989	0.888022	11.20
0.4	0.12	0.999998	0.945122	5.49	0.999999	0.81441	18.56
Position		R = 0.3901			R = 0.8778		
x	*y*	I_{con}	I_{ign}	Difference (%)	I_{con}	I_{ign}	Difference (%)
–0.4	0.12	0.999998	0.548026	45.20	1	0.3927	60.72
–0.3	0.23	0.935226	0.722883	22.70	0.813821	0.621915	23.58
–0.15	0.3	0.999999	0.963633	3.64	0..999999	0.948224	5.18
0	0.32	0.881477	0.83152	5.67	0.809757	0.774136	4.40
0.15	0.3	0.999999	0.963632	3.64	0.999999	0.948224	5.18
0.3	0.23	0.935226	0.72289	22.70	0.813821	0.621921	23.58
0.4	0.12	0.999995	0.548037	45.20	0.999989	0.392764	60.72

4.2. Optimization results

Optimal torque is determined respectively by considering structural stiffness and ignoring structural stiffness. If structural stiffness is ignored, the optimal torque is the same for each case because the maximum driving torque is fixed. However, the stiffness ellipse is not the same for each case because structural stiffness affects the stiffness of end-effector. For accurate torque control, optimization that considers the structural stiffness is necessary.

In Fig. 6, the magenta ellipses show optimal torque considering structural stiffness, and blue ellipses show optimal torque ignoring structural stiffness. Green ellipses show the stiffness ellipse in the non-redundant case. In the non-redundant case, the maximum and minimum stiffness differ significantly. Thus, the directivity of the stiffness is distinct. Optimal results have a more uniform directional stiffness. When R is bigger, the stiffness ellipse is smaller and there is more difference between the results considering structural stiffness and the results ignoring it. This proves that the strength of the linkages is weaker. Structural stiffness is a more important factor in determining the stiffness of the redundant parallel mechanism. Numerical differences for each case are arranged in Table III. I_{con} means index I with optimal toque considering the structural stiffness, and I_{ign} means index I with optimal torque ignoring the structural stiffness. By increasing the dimensionless number R, the error of index I is increased. This research gives instruction that an analysis of structural stiffness is essential in optimizing PKMs with thin linkages.

In the workspace, the difference between I_{con} and I_{ign} is small in the center ($(x, y) = (0, 0.32)$) and large on the side ($(x, y) = (\pm 0.4, 0.12)$). This result denotes that the structural stiffness is relatively small on the side due to the geometric configuration of the 5R PKM. In the center position, the structural stiffness is large due to the symmetric configuration. Note that the structural stiffness was proven to be small at the side, as described in Section 3.3.

5. Conclusion

We presented a stiffness analysis and the optimal torque of a redundantly actuated PKM considering actuator stiffness and structural stiffness. We evaluated the distribution of stiffness by using the ratio of the singular values of a stiffness matrix. The non-redundant case shows the same distribution between actuator stiffness and structural stiffness, so structural stiffness did not affect the characteristic of the actual stiffness significantly. The distribution of structural stiffness is different from the actuator stiffness of the redundant PKM because the redundant PKM had surplus internal torques. In order

https://doi.org/10.1017/S0263574714001209 Published online by Cambridge University Press

to establish the effect of structural stiffness on the actual stiffness, a dimensionless number that indicates the relative strength of the linkages was suggested. The results of optimization show that as the dimensionless number increases, the difference between the optimal torque considering and ignoring the structural stiffness increased. The optimal torque for the case in which we ignore structural stiffness could not produce isotropic stiffness under an actual condition. When PKMs with thin linkages are designed or controlled, the actuator stiffness and structural stiffness need to be analyzed simultaneously.

Acknowledgements

This work was supported by a National Research Foundation (NRF) of Korea grant, funded by the Ministry of Education, Science and Technology (MEST) of the Korean government (NRF-2011-0009596).

References

1. J. P. Merlet, *Parallel Robots*, 2nd ed. (Springer, Dordrecht, the Netherlands, 2006).
2. H.-S. Shim, T. Seo and J. W. Lee, "Optimal torque distribution method for a redundant 3-RRR parallel robot using a geometrical analysis," *Robotica* **31**(4), 549–554 (2013).
3. C. Ahn, T. Seo, J. Kim and T. Kim, "High-tilt parallel positioning mechanism development and cutter path simulation for laser micro-machining," *Comput.-Aided Des.* **39**(3), 218–28 (2007).
4. J. Kim, F. C. Park, S. J. Ryu, J. Kim, J. Hwang, C. Park and C. Iurascu, "Design and analysis of a redundantly actuated parallel mechanism for rapid machining," *IEEE Trans. Robot. Autom.* **17**(4), 423–434 (2001).
5. D. Zhang, "On stiffness improvement of the Tricept machine tool," *Robotica* **23**(3), 377–286 (2005).
6. J. Wu, J. Wang, T. Li and L. Wang, "Performance analysis and application of a redundantly actuated parallel manipulator for milling," *J. Intell. Robot. Syst.* **50**(2), 163–180 (2007).
7. D. Chakarov, "Study of the antagonistic stiffness of parallel manipulators with actuation redundancy," *Mech. Mach. Theory* **39**(6), 583–601 (2004).
8. S. Lee, S. Kim, W. In, M. Kim, J. I. Jeong and J. Kim, "Experimental verification of antagonistic stiffness planning for a planar parallel mechanism with 2-DOF force redundancy," *Robotica* **29**(4), 547–554 (2011).
9. Y. Xu, J. Yao and Y. Zhao, "Inverse dynamics and internal forces of the redundantly actuated parallel manipulators," *Mech. Mach. Theory* **51**, 172–184 (2012).
10. P. Limaye, G. Ramu, S. Pamulapati and G. K. Ananthasuresh, "A compliant mechanism kit with flexible beams and connectors along with analysis and optimal synthesis procedures," *Mech. Mach. Theory* **49**, 21–39 (2012).
11. A. Rezaei, A. Akbarzadeh and M.-R. Akbarzadeh-T., "An investigation on stiffness of a 3-PSP spatial parallel mechanism with flexible moving platform using invariant form," *Mech. Mach. Theory* **51**, 195–216 (2012).
12. H. Shin, S. Lee, W. In, J. I. Jeong and J. Kim, "Kinematic optimization of a redundantly actuated parallel mechanism for maximizing stiffness and workspace using Taguchi method," *J. Comput. Nonlinear Dyn.* **6**(1) (2011).
13. X.-J. Liu, Z.-L. Jin and F. Gao, "Optimum design of 3-DOF spherical parallel manipulators with respect to the conditioning and stiffness indices," *Mech. Mach. Theory* **35**(9), 1257–1267 (2000).
14. X.-J. Liu, J. Wang and G. Pritschow, "Kinematics, singularity and workspace of planar 5R symmetrical parallel mechanisms," *Mech. Mach. Theory* **41**(2), 145–169 (2006).
15. R. S. Goncalves, J. C. M. Carvalho, G. Carbone and M. Ceccarelli, "Indices for stiffness and singularity evaluation for designing 5R parallel manipulator," *Open Mech. Eng. J.* **4**, 61–68 (2010).

https://doi.org/10.1017/S0263574714001209 Published online by Cambridge University Press